HHS Public Access

Author manuscript

Nat Struct Mol Biol. Author manuscript; available in PMC 2018 February 26.

Published in final edited form as:

Nat Struct Mol Biol. 2016 May ; 23(5): 434–440. doi:10.1038/nsmb.3202.

SIRT6 deacetylates H3K18Ac at pericentric chromatin to prevent mitotic errors and cell senescence

Luisa Tasselli[1,2], **Yuanxin Xi**[3], **Wei Zheng**[1,2], **Ruth I. Tennen**[1], **Zaneta Odrowaz**[1,2], **Federica Simeoni**[1,2], **Wei Li**[3], and **Katrin F. Chua**[1,2]

[1]Department of Medicine, Stanford University School of Medicine, Stanford, California, USA

[2]Geriatric Research, Education, and Clinical Center, Veterans Affairs Palo Alto Health Care System, Palo Alto, California, USA

[3]Department of Molecular and Cellular Biology, Baylor College of Medicine, Houston, Texas, USA

Abstract

Pericentric heterochromatin silencing at mammalian centromeres is essential for mitotic fidelity and genomic stability. Defective pericentric silencing is observed in senescent cells, aging tissues, and mammalian tumors, but the underlying mechanisms and functional consequences of these defects are unclear. Here, we uncover a pivotal role of the human SIRT6 enzyme in pericentric transcriptional silencing, and show that this function protects against mitotic defects, genomic instability, and cellular senescence. At pericentric heterochromatin, SIRT6 promotes deacetylation of a new substrate, histone H3 lysine K18 (H3K18), and inactivation of SIRT6 in cells leads to H3K18 hyperacetylation and aberrant accumulation of pericentric transcripts. Strikingly, RNAi-depletion of these transcripts rescues the mitotic and senescence phenotypes of SIRT6-deficient cells. Together, our findings reveal a new function for SIRT6 and H3K18Ac regulation at heterochromatin, and demonstrate the pathogenic role of de-regulated pericentric transcription in aging- and cancer- related cellular dysfunction.

Large-scale chromatin changes occur during aging, cancer, and other disease processes [1–5]. The mammalian chromatin regulatory factor SIRT6, a member of the sirtuin family of NAD$^+$ (nicotinamide adenine dinucleotide)-dependent enzymes, has pivotal roles in aging, metabolism, and cancer biology [6]. SIRT6-deficiency in mice leads to severe metabolic defects, genomic instability, inflammatory disease, and accelerated tumorigenesis [7–12],

Correspondence should be addressed to K.F.C (kfchua@stanford.edu) and W.L. (WL1@bcm.edu).

AUTHOR CONTRIBUTIONS

L.T. and K.F.C conceived the project, designed the experiments and wrote the manuscript. L.T. performed *in vitro* and cellular deacetylation assays, ChIP and ChIP-seq experiments, RNA expression analysis, microscopy, and cell biology experiments. Y.X. and W.L. performed bioinformatic analyses for the ChIP-seq experiments and contributed to the corresponding manuscript sections. W.Z. performed ChIP experiments in KAP1 depleted cells and contributed to analysis of KAP1 in SIRT6 depleted cells. R.I.T. contributed to the deacetylation assay on H3K18Ac peptides, analysis of satellite transcripts, and manuscript editing. Z.O. performed ChIP experiments in SIRT6 overexpressing cells. F.S. purified nucleosomes for deacetylation assays.

ACCESSION CODES

Gene Expression Omnibus

GSE69809

whereas overexpression of SIRT6 can extend mouse lifespan [13]. Notably, down-regulated SIRT6 expression is observed in human cancers [10,14,15], and is associated with advanced donor age in primary human fibroblasts [16]. Thus, deciphering the molecular functions of SIRT6 should contribute to elucidating fundamental mechanisms of aging and disease biology. Many functions of SIRT6 are linked to its activity at chromatin, where it catalyzes NAD^+-dependent deacetylation of histone H3 on H3K9Ac and H3K56Ac (acetylated lysines K9 and K56 of histone H3, respectively) [17–19]. SIRT6 associates with telomeric chromatin, where it prevents telomere instability, replicative cellular senescence, and impaired silencing of telomere-proximal genes [17,20]. At promoters of active genes, SIRT6 represses gene networks associated with aging, metabolism, and tumor progression [8,10,12,21,22]. SIRT6 also coordinates nuclear responses to DNA damage by stabilizing the association of DNA repair and chromatin remodeling factors at DNA breaks [23,24], and by regulating the activity of DNA processing and repair factors [25,26]. Notably, in addition to deacetylating histone H3, SIRT6 can also deacetylate non-histone proteins [25,27], and catalyze mono-ADP-ribosylation [26,28] and deacylation of long-chain fatty acyl groups [29]. Thus, elucidating the different enzymatic activities and substrates of SIRT6 that are linked to distinct genomic contexts and cellular processes should provide important insights into chromatin and nuclear signaling mechanisms.

Constitutive heterochromatin is present at non-coding regions of the genome and functions to silence transcription or genomic rearrangement of repetitive DNA elements. A classic example of constitutive heterochromatin is pericentric heterochromatin at mammalian centromeres, which occurs at arrays of tandem satellite (Sat) DNA repeat elements (mainly Sat II and Sat III) that are enriched for GGAAT motifs [30,31]. Notably, de-regulated transcription of pericentric satellite repeats occurs in pancreatic and other cancers [3], and is associated with premature and physiologic aging of mammalian cells and tissues [1,2,4]. However, it is not yet known whether these pericentric silencing defects have a causal role in triggering cellular dysfunction associated with cancer and aging.

In this study, we set out to identify new mechanisms of chromatin regulation by SIRT6 and characterize their importance for cellular function. We show that SIRT6 maintains pericentric heterochromatin silencing at human centromeres through deacetyation of a novel substrate, and this activity is important for protecting against mitotic errors, genomic instability, and cellular senescence.

RESULTS

H3K18Ac is a physiologic SIRT6 substrate

We previously carried out *in vitro* screens for NAD^+-dependent SIRT6 deacetylase activity on a set of acetylated histone peptides by mass spectrometry [17,18]. Upon extending this analysis to new peptides, we found that SIRT6 robustly deacetylated lysine K18 on histone H3 peptides (H3K18Ac) (Fig. 1a). SIRT6 also efficiently deacetylated H3K18Ac on nucleosome substrates, whereas a catalytically inactive SIRT6 mutant protein (H133Y) did not (Fig. 1b). By contrast, H3K18 deacetylation by SIRT6 was much less efficient on free histone H3 than on the nucleosome substrates (Supplementary Fig. S1a). This observation suggests that the physiologic role of SIRT6 in H3K18Ac deacetylation occurs in the context

of chromatin, as previously reported for its H3K9Ac and H3K56Ac deacetylase activities [32]. SIRT6 also promoted H3K18Ac deacetylation when over-expressed in cells, while the mutant SIRT6 H133Y protein did not (Fig. 1c). Finally, global H3K18Ac levels were increased in SIRT6-deficient mouse embryonic fibroblasts (MEFs), and reconstitution with wild-type murine SIRT6, but not the catalytically inactive SIRT6 H133A protein, restored H3K18Ac deacetylation (Fig. 1d, e, Supplementary Fig. S1b). Together, these data identify H3K18Ac as a new chromatin substrate of SIRT6, and demonstrate a physiologic role of SIRT6 in maintaining total cellular levels of this histone mark.

SIRT6 promotes H3K18 deacetylation at pericentric chromatin

To determine how SIRT6 affects the genomic landscape of H3K18Ac, we carried out unbiased ChIP-sequencing (ChIP-seq) in SIRT6-depleted or control U2OS osteosarcoma cells. Genome-wide analysis of the H3K18Ac ChIP-seq peak profiles revealed that in the SIRT6-deficient cells, H3K18Ac occupancy was dramatically increased (p-value: 9×10^{-20}) at pericentric regions (average signal at peaks within ~100Kb of centromere “gaps”, where sequence is missing from annotated genomes) (Fig. 2a,b). H3K18Ac hyperacetylation was also clear at individual pericentric, but not sub-telomeric, regions (Fig. 2c). By contrast, although pericentric H3K9Ac and H3K56Ac levels were subtly increased in the SIRT6-depleted cells, these changes were much less substantial than observed for H3K18Ac (Supplementary Fig. S2b). Surprisingly, although SIRT6 binds and deacetylates H3K9Ac and H3K56Ac at sub-telomeric regions and transcription start sites (TSS’s) [10,17,18,20,21], SIRT6 inactivation did not significantly alter H3K18Ac levels at these sequence elements, at least at the genome-wide level of this analysis (Fig. 2a, Supplementary Fig. S2a).

In an independent approach, we aligned the H3K18Ac ChIP-seq reads to consensus sequences of pericentric repeats [30], as well as other repetitive DNA element families. SIRT6-depleted cells showed increased H3K18Ac levels at pericentric sequences, but not at telomeric and other repeat sequences (Fig. 2d, Supplementary Fig. S2c). Moreover, H3K18Ac levels were also not robustly altered at multiple chromosome-specific and consensus α-Satellite sequences at centromeric core regions [30] (Supplementary Fig. S2d). Thus, the effects of SIRT6 on H3K18Ac levels appear to be specific to pericentric satellite sequences.

Direct ChIP-qPCR confirmed the ChIP-seq findings, and revealed a robust increase in H3K18Ac levels at pericentric satellite repeats in SIRT6-depleted cells (Fig. 2e), and deacetylation of pericentric H3K18Ac in cells overexpressing recombinant wild type SIRT6 but not catalytically inactive SIRT6 H133Y protein (Fig. 2f, Supplementary Fig. S2e). We also confirmed that the effects of SIRT6 activity at pericentric heterochromatin are specific for H3K18Ac, as H3K9Ac and H3K56Ac ChIP signals were not reproducibly altered at pericentric or centromere core sequences, after either overexpression or depletion of SIRT6 (Supplementary Figs. S2f, g). Together, these data indicate that SIRT6 promotes site-specific deacetylation of H3K18Ac at centromeres, but not at its other known genomic targets.

SIRT6 promotes pericentric heterochromatin silencing

We next examined the association of SIRT6 protein with pericentric satellite DNA sequences by ChIP-qPCR. SIRT6 occupancy was specifically enriched at Sat II and Sat III sequences. Importantly, the ChIP signal was reduced in SIRT6-depleted cells, demonstrating the specificity of the SIRT6 ChIP (Fig. 3a and Supplementary Fig. S3a). We also observed the interaction of SIRT6 with centromeres by co-immunoprecipitation of the centromere-specific marker CENP-A [31] with SIRT6 (Fig. 3b) and by co-localization of SIRT6 with CENP-A by confocal microscopy (Fig. 3c).

To examine the functional importance of H3K18 deacetylation by SIRT6, we compared levels of pericentric satellite transcripts in SIRT6-depleted and control U2OS cells by qRT-PCR. SIRT6-deficient cells exhibited markedly increased levels of Sat II and Sat III transcripts, while negative control 5S ribosomal RNA levels were unaltered. By contrast, only minimal changes were observed at α-Sat transcripts, and these might reflect indirect effects of the pericentric chromatin alterations on adjacent centromere core sequences (Fig. 3d). We also confirmed the increase in pericentric satellite transcripts in SIRT6-depleted cells by Northern blot analysis, which revealed transcripts ranging in size from <1kb to >9Kb in nuclear, but not cytoplasmic, RNA fractions (Supplementary Fig. S3b), similar to previous observations for human Sat III transcripts induced by heat shock [33]. Consistent with the de-repressed pericentric transcription, Sat II and Sat III sequences in the SIRT6-deficient cells also exhibited increased levels of activated RNA Pol II (RNA Polymerase II phosphorylated at Ser2) and H3K36me3 (histone H3 lysine K36 tri-methyl), a marker of active transcription (Fig. 3e and Supplementary Fig. S3d). Together, these data suggest that SIRT6 is important for maintaining transcriptional repression at pericentric heterochromatin.

Surprisingly, however, the dramatic loss of satellite transcript silencing was not accompanied by clear decreases in H3K9me3 or HP1α, typical markers of silent heterochromatin, in both ChIP-qPCR or unbiased ChIP-seq assays (Fig. 3f and Supplementary Fig. S3e, f). This contrasts with the almost complete loss of H3K9me3 previously shown to be associated with pericentric heterochromatin silencing defects in cells doubly deficient for the H3K9me3 methyltransferase enzymes Suv39H1 and Suv39H2 [34,35]. Thus, our data suggest that H3K18 deacetylation by SIRT6 silences transcription at pericentric heterochromatin by a mechanism that is at least partly independent of or downstream of the H3K9me3–HP1α heterochromatin maintenance pathway.

We next considered possible mechanisms for how regulation of pericentric H3K18Ac levels by SIRT6 could lead to changes in satellite repeat transcription. Recent work reported that SIRT6 promotes transcriptional silencing at LINE-1 retrotransposable elements by regulating the transcriptional repressor protein KAP1 [28]. Although KAP1 has been detected at pericentric chromatin [36,37], to our knowledge, a role for KAP1 in pericentric satellite repeat silencing has not been reported. KAP1 contains a C-terminal PHD finger–bromodomain module that is found on many chromatin-associated transcriptional regulatory proteins. Interestingly, while bromodomains generally bind acetylated lysines, the KAP1 bromodomain lacks several conserved residues that mediate acetyl-lysine binding and does not bind multiple acetyl-lysine peptides [38]. Consistent with these observations, we found that the KAP1 protein (both endogenous and recombinant) bound specifically to unmodified

histone H3 peptides, whereas acetylation on H3K18 disrupted this interaction (Fig 3g, h). As a control, the AF9 YEATS domain bound the H3K18Ac but not the unmodified peptide, as previously shown [39]. This observation suggested that deacetylation of H3K18Ac by SIRT6 may be important for KAP1 retention at pericentric satellite repeats, and in the absence of SIRT6, H3K18 hyperacetylation triggers KAP1 release and transcriptional de-repression. Further supporting this model, we found that inactivation of SIRT6 in cells specifically reduced KAP1 occupancy at pericentric satellite repeats (Fig. 3i; Supplementary Fig. S3g,h). Importantly, depletion of KAP1, similar to depletion of SIRT6, led to increased satellite transcript expression without affecting H3K9me3 levels (Fig. 3j; Supplementary Fig. S3i, j). Together, these findings suggest a novel mechanism in pericentric transcriptional silencing, in which SIRT6-dependent changes in acetylation state at H3K18 are “read” by acetylation-sensitive binding of a known transcriptional repressor.

Pathologic pericentric transcripts trigger cellular defects

Although pericentric repeat sequences are largely transcriptionally repressed, low-level transcription of satellite DNA transcripts has crucial roles in the assembly and function of pericentric heterochromatin itself [40–42]. However, the observation that de-regulated transcription of pericentric transcripts is detected in aging and cancer has led to the suggestion that aberrant accumulation of these transcripts might have pathogenic consequences. Here, we examined the functional consequences of pericentric satellite transcript accumulation in SIRT6-deficient U2OS cells. Confocal microscopy revealed dramatically increased (>25%) abnormal mitoses in the SIRT6-deficient cells with multipolar spindles and supernumerary centrosomes (Fig. 4a–c), as well as disorganized or asymmetric mitoses (Supplementary Fig. S4a). Moreover, the SIRT6-depleted cells exhibited increased chromosome mis-segregation and aneuploidy, as detected using a chromosomal instability assay for aneuploidy [43] that quantifies centromere-containing micronuclei (cytoplasmic bodies containing DNA that is lost from nuclei during anaphase) (Fig. 4d, Supplementary Fig, S4b). These observations indicate that SIRT6 protects against genomic instability associated with chromosome segregation errors during mitosis.

We next asked whether the mitotic defects in SIRT6-deficient cells are dependent on impaired pericentric heterochromatin silencing, rather than other effects of SIRT6 loss. Strikingly, depletion of the Sat III transcripts in SIRT6-deficient U2OS cells by siRNA-mediated RNA interference [33] markedly reversed the mitotic defects in these cells (Fig. 4e, Supplementary Fig. S4c). This rescue could not result from non-specific siRNAs effects, because mitotic defects were not reduced by the Sat III siRNAs in SIRT6-proficient control cells (Fig. 4e). These findings demonstrate that the aberrant accumulation of satellite transcripts in SIRT6-deficient cells has a pathogenic role in triggering mitotic dysfunction.

Increased levels of pericentric satellite transcripts are observed in senescent human fibroblasts, cells from human progeroid patients, and tissues from aged mice [1,2,4], suggesting that deregulated satellite transcription might contribute to cellular senescence or other aging-related cellular dysfunction. In addition, cellular senescence could be triggered by mitotic defects as a tumor suppressive response in cancer cells, to prevent propagation of potentially oncogenic genomic changes. We previously showed that SIRT6 loss in primary

human fibroblasts leads to premature replicative cellular senescence during long-term serial passaging, due to telomere dysfunction [17]. However, the effect of SIRT6 inactivation on senescence of cancer cells such as U2OS osteosarcoma cells (which do not undergo telomere-dependent replicative senescence) has not been described. We detected significantly increased numbers of senescent U2OS cells (over ~20-fold higher than control cells) within a week of SIRT6 depletion by lentiviral shRNAs (Fig. 4f,g), and increased senescence was observed as early as 72 hours after transient transfection of SIRT6 siRNAs (Fig. 4h and Supplementary Fig. S4d). The acute nature of the observed cellular senescence suggests that it occurs via a different mechanism than the previously described telomere-dependent replicative senescence in primary human fibroblasts [17]. Indeed, we did not observe signs of telomere dysfunction in SIRT6-depleted U2OS cells in this acute time-frame (data not shown), consistent with previous results [20]. Moreover, like the mitotic errors, the senescence phenotype of SIRT6-depleted cancer cells was rescued by depletion of the Sat III transcripts (Fig. 4h and Supplementary Fig. S4c, d). Notably, demonstrating the generality of our findings, the increased levels of Sat III transcripts and associated cellular senescence were also observed following depletion of SIRT6 in other cancer cell lines (HeLa and A549 cells) (Supplementary Figure S4f), and depletion of Sat III transcripts in A549 cells reversed this senescence (Supplementary Figure S4g). Finally, we found that ectopic expression of Sat III transcripts in U2OS cells led to increased levels of senescence (Supplementary Figure S4e), and previous work showed that overexpression of satellite transcripts leads to increased abnormal mitoses [44]. Thus, the data indicate that pathologic accumulation of pericentric satellite transcripts can be both necessary and sufficient for inducing mitotic errors and acute cellular senescence. We conclude that H3K18 deacetylation and pericentric chromatin silencing by SIRT6 protect against mitotic errors and cellular senescence by preventing transcription of pathogenic satellite DNA elements.

DISCUSSION

Here, we have identified H3K18Ac as a new SIRT6 substrate, and shown that SIRT6 has a highly specific and limiting role in determining H3K18Ac levels at pericentric heterochromatin. We show that depletion of SIRT6 in U2OS cancer cells leads to dramatic site-specific hyperacetylation of H3K18 and pathologic de-regulated transcription at pericentric satellite repeat elements. These observations suggest important, previously unappreciated roles of SIRT6 and H3K18 deacetylation in maintaining pericentric heterochromatin silencing.

H3K18Ac is enriched at promoters of active genes [45], and we previously showed that SIRT7, a member of the sirtuin family closely related to SIRT6, selectively deacetylates H3K18Ac at a subset of these promoters to regulate expression of genes involved in maintenance of oncogenic transformation [46]. By contrast, our ChIP-seq experiments revealed few promoters with increased H3K18Ac levels (data not shown) in SIRT6-deficient cells. These observations suggest that SIRT6-dependent deacetylation of H3K18Ac may not have a large role in gene repression, at least under basal conditions. However, it remains possible that SIRT6-dependent deacetylation of H3K18Ac might occur at specific genes under certain conditions, such as under stress or to compensate for physiologic or induced decreases in SIRT7 levels. In contrast to our findings for SIRT6, SIRT7-deficient cells did not exhibit

increased levels of pericentric H3K18Ac or pericentric satellite transcripts (Supplementary Fig. S3c; **data not shown)**. These observations suggest that SIRT6 and SIRT7 have distinct functions in maintaining deacetylation of H3K18Ac at gene promoters versus constitutive heterochromatin. Similar to SIRT6, the sirtuin SIRT1 localizes at pericentric heterochromatin, and it contributes to pericentric satellite repeat silencing in mouse embryonic stem (ES) cells [47]. However, de-repression of pericentric satellite transcripts was not seen in SIRT1 deficient ES cells, and it was proposed that other deacetylase enzymes may compensate for SIRT1 in pericentric heterochromatin silencing [47]. It is possible that SIRT6 might provide such a compensatory function.

Previous studies of pericentric heterochromatin maintenance have linked derepression of satellite transcription to dramatic or complete loss of pericentric H3K9me3, due to combined inactivation of the H3K9me3 methyltransferases Suv39H1 and Suv39H2 [34,35], or the H3K9me1 methyltransferases Prdm3 and Prdm16 [48]. Similarly, increased satellite transcript accumulation in human mesenchymal stem cells, due to depletion of the Werner syndrome factor WRN, was recently linked to abolishment of pericentric H3K9me3 levels [49]. By contrast, our studies show that in SIRT6-depleted cells, dramatic increases in pericentric satellite transcript levels are associated with only subtle or negligible alterations in pericentric H3K9me3. These observations suggest that maintenance of pericentric heterochromatin silencing by SIRT6 and H3K18Ac deacetylation may constitute a novel mechanism, which is independent of the classic H3K9me3 heterochromatin maintenance pathway. Consistent with this possibility, previous studies have reported observations similar to ours, where increased satellite DNA transcription occurs without dramatic H3K9me3 changes. For example, inhibition of DNA methylation in MEFs by 5-Aza-2′-deoxycytidine treatment increases pericentric satellite transcription without altering pericentric H3K9me3 and HP1 levels [50]. Our data are also consistent with models in which SIRT6 functions downstream of the H3K9me3–HP1 pathway, as has been reported in *S. pombe*, where transcriptional silencing of centromeric repeats involves recruitment of a histone deacetylase that acts downstream of H3K9me3 [40].

In this study, we provide evidence for a novel mechanism through which SIRT6-dependent changes in H3K18 acetylation may contribute to pericentric transcriptional silencing. In this model, changes in acetylation state at H3K18 are “read” by acetylation-sensitive binding of the transcriptional co-repressor KAP1 [38]. We show that KAP1 specifically binds unmodified histone H3 sequences, whereas acetylation on H3K18 disrupts this interaction. Moreover, KAP1 associates with pericentric satellite sequences, but in SIRT6-deficient cells, H3K18 hyperacetylation triggers KAP1 release and transcriptional de-repression.

We note that our data do not exclude that other mechanisms might also contribute to the silencing function of SIRT6 at satellite repeats. For example, previous work showed that SIRT6 promotes heterochromatic silencing at LINE1 retrotransposable elements by ADP-ribosylating KAP1, which stabilizes the repressive KAP1–HP1α complex at these elements. It is possible that KAP1 ribosylation by SIRT6 might also contribute to pericentric heterochromatin silencing. However, at LINE1 elements, loss of silencing in the absence of SIRT6 is associated with drastic reductions in H3K9me3 and HP1α levels, which we did not observe at pericentric heterochromatin. Moreover, in our ChIP-sequencing experiments,

SIRT6 did not significantly affect H3K18Ac levels at endogenous LINE1 elements (Supplementary Fig. S2C). Thus, SIRT6 and KAP1 may employ distinct mechanisms to promote heterochromatin silencing at pericentric satellites versus L1 retrotransposons. At pericentric heterochromatin, this mechanism is either independent of or downstream of H3K9me3 changes. Interestingly, KAP1 has been reported to regulate Pol II pausing, and KAP1 depletion leads to increased active transcriptional elongation at numerous genes [51]. Thus, it is possible that the mechanism of SIRT6 and KAP1 in pericentric transcriptional silencing may involve regulation of Pol II pausing.

Growing evidence indicates that heterochromatin breakdown and accumulation of pericentric satellite transcripts occur in senescent cells, aging tissues, and human cancers [1–4], but whether the silencing defects have a causal role in triggering cellular dysfunction in these contexts has not been determined. Here, we have shown that pericentric heterochromatin defects in SIRT6-deficient cells lead to mitotic errors, genomic instability, and acute cellular senescence, and remarkably, these defects are rescued by depletion of the pericentric transcripts. These findings demonstrate that the pathologic accumulation of satellite transcripts is a cause, rather than consequence, of aging- and cancer- related cellular dysfunction. This conclusion is supported by the observation that ectopic expression of satellite transcripts can induce senescence (Supplementary Fig. S4g) and mitotic defects[44].

Similar to our observations with SIRT6-depleted cells, cells from patients with Hutchinson-Gilford Progeria Syndrome (HGPS) also exhibit pericentric heterochromatin defects and satellite transcript accumulation, and undergo premature cellular senescence [4]. Intriguingly, a recent study reported that SIRT6 is down-regulated in HGPS cells, and SIRT6 overexpression in these cells can rescue their senescence phenotype [52]. The mechanism by which this occurs is still unknown, but it is tempting to speculate that it could involve, at least in part, re-silencing of pericentric transcripts by SIRT6. Together, our study uncovers a new mechanism and molecular substrate through which SIRT6 protects against cellular dysfunction associated with aging and cancer.

ONLINE METHODS

Cell culture, over-expression and RNA interference

Human 293T and U2OS cell lines (ATCC) were cultured in MEM supplemented with 10% FBS, 2mM L-Glutamine and Pen/Strep. HeLa and A549 cells (ATCC) were cultured in DMEM with 10% FBS, 2mM L-Glutamine and Pen/Strep. MEFs were generated from 13.5-day-old WT and SIRT6 KO mouse embryos using standard methods as previously described [7]. MEFs were grown in Advanced DMEM supplemented with 10% FBS, 2mM L-Glutamine, 0.1mM 2-mercaptoehanol and Pen/Strep. MEFs were propagated by described 3T3 protocols for spontaneous immortalization [53]. Stable SIRT6, SIRT7 and KAP1 knockdown and SIRT6 knockout cells were generated by lentiviral transduction. For lentiviral packaging, 293T cells were co-transfected with pVPack-VSV-G, Δ8.2 and pSicoR containing shRNAs directed against SIRT6, SIRT7, KAP1 or control constructs, or LentiCRISPRv2 containing guide RNA directed towards SIRT6 gene or Luciferase control, and viral supernatant was collected after 48 h. For transduction, cells were incubated with

virus-containing supernatant in the presence of 8 μg/ml polybrene. After 48 h, infected cells were selected for 72 h with puromycin (1.5 μg/ml).

Target sequences were as follows:

SIRT6 KD1 5′-AAGAATGTGCCAAGTGTAAGA- 3′;

SIRT6 KD2 5′-AAAGTCCTCAATGCAATAA- 3′.

SIRT7 KD 5′-CACCTTTCTGTGAGAACGGAA- 3′ as previously described [46]

KAP1 KD 5′ –GTGCAACCAGTGTGAGTTT- 3′

For CRISPR SIRT6 deletion, guide RNA was directed towards SIRT6 target sequence:

CCTCCCGGAGGTGAGCGCGTCTG

U2OS cells stably expressing Sat III were generated by lentiviral transduction, as described for SIRT6 knockdown. A previously described Satellite III sequence [54] of 131bp containing repeats of (GGAAT)*n* CAAC(C/A)CGAGT or *v*ariations of this module was cloned into p156RRL-EF1a-GFPU3H1 lentiviral vector used for lentiviral packaging.

U2OS cells and MEFs stably expressing Flag-tagged human or mouse SIRT6 and SIRT6 catalytic mutants (human H133Y or mouse H133A) were generated by retroviral transduction. For retroviral packaging, 293T cells were co-transfected with pVPack-VSV-G, pVPack-GP and pBabe vectors containing SIRT6, SIRT6 catalytic mutant or empty vector. Retroviral transduction and selection were performed as for lentiviral transduction.

siRNA transfections were performed using Dharmafect reagent (Dharmacon), according to the manufacturer's instructions and with the following target sequences:

siRNA control 5′-TGGTTTACATGTCGACTAA- 3′;

siRNA SIRT6 (siS6) 5′-GAATGTGCCAAGTGTAAGA- 3′;

siRNA Satellite III (siSat III) 5′-TGGAATGGAATGGAATGGA- 3′ as previously described [33].

Antibodies

List of antibodies used in this study is provided in Supplementary Table S1. Validation of each primary antibody is provided on the manufacturers' websites or in ref. [55].

Histone deacetylation assays and mass spectrometry

In vitro histone deacetylation assays were performed as described previously, with minor modifications [17]. Briefly, 2μg of recombinant SIRT6 and 0.4 μg of acetylated histone tail peptide or full-length calf thymus histone H3 (Roche) or 0.5 μg mononucleosomes purified from HeLa cells, were incubated in HDAC buffer (50 mM Tris-HCl pH 8.0, 2 mM NAD+, 150 mM NaCl) for 4 h at 30 °C. The reaction mixture was analyzed by western blot or mass spectrometry analysis.

Purification of human SIRT6 protein from baculovirus-infected insect cells was described previously [55]. Histone peptides were synthesized at the Yale W. M. Keck peptide synthesis

facility, and liquid chromatography mass spectrometry was performed at the Stanford University, Protein and Nucleic Acid Facility.

To determine histone acetylation levels in cells, 293T and U2OS cells were transiently transfected with pcDNA3 or pBabe vectors containing Flag-tagged wild-type SIRT6, the SIRT6-HY catalytic mutant or an empty vector. Whole-cell lysates were collected after 48h. Western blot analysis of histone acetylation levels was performed with modification-specific antibodies listed in Supplementary Table S1.

Immunofluorescence

Cells were fixed with 4% paraformaldehyde, washed, permeabilized with 0.1% Triton X-100 for 10 min, blocked with 2% bovine serum albumin/PBS and immunostained with antibodies listed in Supplementary Table S1. For analysis of SIRT6 co-localization with CENP-A, U2OS cells were transiently transfected with pEGFP-N2-Flag SIRT6, detergent extracted to remove nucleoplasmic proteins with Triton X-100 buffer (0.5% Triton X-100, 20 mM Hepes-KOH pH 7.9, 50 mM NaCl, 3 mM MgCl2, 300 mM sucrose) for 5 min at 4°C, washed in PBS, and fixed in 3% paraformaldehyde, 2% sucrose in PBS for 10 min at room temperature. Cells were then re-permeabilized, blocked, and immunostained for CENP-A as described above. Coverslips were mounted using ProLong Gold Antifade reagent with DAPI (Invitrogen) and imaged using a Zeiss LSM700 confocal laser-scanning microscope.

Co-immunoprecipitation

Cells were harvested, washed in PBS, and suspended in cell lysis buffer [10 mM Hepes (pH 7.5/7.9), 0.34 M sucrose, 10% glycerol, 10 mM KCl, 1.5 mM MgCl2, protease inhibitors] containing 0.2% NP-40 and kept on ice for 20 min. Cell extracts were centrifuged at 800 × g for 10 min at 4°C to separate the nuclear pellet from the cytoplasm. The nuclear pellet was suspended in cell lysis buffer containing 2 mM CaCl2 and kept 10 min at room temperature. Nucleosomes were prepared by digestion with micrococcal nuclease (10 U/mL) at 37°C for 5 min. The reaction was terminated by addition of 2 mM EGTA and 200 mM KCl (final concentrations), incubated 10 min at 4°C, and centrifuged at 16,000 × g for 30 min to separate the insoluble chromatin pellet from the soluble chromatin fraction. The soluble chromatin was incubated with anti-Flag M2 agarose beads (Sigma) for immunoprecipitation. Elution was performed by boiling the beads in Laemmli loading buffer.

Chromatin immunoprecipitation (ChIP)

ChIP for SIRT6, KAP1 and RNA Pol II (phosphorylated at Ser2) was performed according to standard protocols (Upstate Biotechnology, Lake Placid, NY) with minor modifications. Briefly, cells were cross-linked with 1% formaldehyde at room temperature for 20 min, quenched with 1.25 M glycine, washed in ice-cold PBS and lysed with SDS lysis buffer [1% SDS, 10 mM EDTA, 50 mM Tris-HCl (pH 8)]. Cellular lysates were sonicated, diluted with ChIP dilution buffer [SDS 0.01%, 1.1% Triton X-100, 1.2 mM EDTA, 16.7 mM TrisHCl, 167 mM NaCl], and immunoprecipitated with primary antibody listed in Supplementary Table S1. Rabbit anti-mouse IgG were used as a negative control. Immunoprecipitates were collected with protein A/G-agarose beads (Thermo Scientific) and washed sequentially with

a low-salt and high-salt wash buffer (Upstate Biotechnology). DNA-protein complexes were eluted in elution buffer [1% SDS and 0.1 M $NaHCO_3$], heated to 65°C overnight, and deproteinized by treatment with proteinase K at 45°C for 1 h.

ChIP of histone marks was performed as previously described [56], using antibodies as in Supplementary Table S1. Rabbit IgG antibody was used as negative control in all the experiments. After elution, DNA was washed and recovered using a PCR purification kit (Qiagen) and assayed by RT-PCR on a LightCycler 480 using SYBR green Master Mix. Fold enrichment was calculated as % input and normalized to total H3. Sequences of primers for centromeric core regions (17a, 21a, 21b, Xa), pericentric Satellite II, 5S Ribosomal DNA regions, and LINE1 elements are previously described [28,57]. Sequences of other primers used are listed in Supplementary Table S2. The efficiency of the primers used for RT-PCR was verified by standard curve to be >90%. For repetitive regions, the immunoprecipitated DNA was diluted at least 10 fold, so that the qPCR data were within the linear range of amplification for each primer. The ChIP signals were then normalized to the input samples; this calculation controls for any variability in amount of chromatin used and any potential differences in number of repetitive elements.

ChIP-sequencing and computational analysis

ChIP for H3K18Ac, H3K9Ac, H3K56Ac, and H3K9me3 were performed as described above, and DNA samples were used for ChIP-sequencing analysis. Sequencing libraries were prepared using the Illumina TruSeq DNA Sample Preparation Kit according to the manufacturer's protocol. DNA fragments were gel purified, PCR amplified, and sequenced using paired-end sequencing technology on Illumina HiSeq 2000 platform. Two independent biological replicates of H3K18Ac ChIP-seq showed similar results.

For ChIP-sequencing profile generation and peak calling, raw reads were aligned to human genome hg19 using bowtie2 v2.1.0 pair-end mapping mode, with parameters "-k 10 --non-deterministic" to allow up to 10 non-unique mappings per reads [58]. The mapping output was processed to randomly select only one alignment per reads pair. Whole genome ChIP-seq profile was generated using DANPOS v2.2.2 [59]. The ChIP-seq peaks were called using the DANPOS "dpos" mode to identify peaks at nucleosome resolution. The pericentric and telomeric peak profiles were generated by averaging all peaks within a 100KB neighborhood of centromeric and telomeric regions. The centromere and telomere location were obtained from cytoband table and gap table in UCSC genome database. For pericentric (PCT) and centromeric (CT) mapping, PCT and CT consensus or chromosome-specific sequences and control sequences were obtained from Eymery et al [30]. A telomeric $(TTAGGG)_8$ sequence was also analyzed as control. Since these sequences are shorter than the sequencing read length (101bp), the number of reads that contain the analyzed sequences were counted, allowing up to 2 mismatches. The read counts for each sample were normalized to unit of reads per million total reads [RPM = reads count / (total_reads / 1,000,000)].

For RepeatMasker mapping, the annotated Repbase repeat family elements were downloaded from UCSC database. The total number of nucleotides that overlapped with each repeat family region was counted and normalized to nucleotide per kilo base-pair per

million reads [NPKM = overlapped nucleotide count / total size of repeat regions / (total reads / 1,000,000)].

RT-PCR

Total RNA was extracted from cells with TRIzol (Invitrogen), following the manufacturer's protocol. Subsequently, the RNA was treated with RQ1 DNase I (Promega) for 30 min at 37°C, to remove any contaminating DNA. Total RNA (0.5 μg) was reverse transcribed using the SuperScript III first-strand synthesis system for RT-PCR (Invitrogen) with random primers or with a specific primer for Sat III, as previously described [54]. Real-time qPCR for SIRT6 expression levels were assayed by using TaqMan Gene Expression Assay, Applied Biosystem. For all other transcripts, RT-qPCR was performed using the SYBR green master mix and LightCycler 480 II. Relative mRNA levels were normalizing to β-actin, GAPDH or 5S Ribosomal RNA expression. Sequences of primers for Sat II, Sat III, α-Sat expression are previously described [1,54,60]. Sequences of all primers used are listed in Supplementary Table S2.

Senescence-associated β-galactosidase assay

Senescence-associated β-galactosidase activity [61] was detected with the Senescence Cells Histochemical Staining Kit (Sigma-Aldrich) according to the manufacturer's instructions. Cells were scored using a Leica DM5000B microscope.

Peptide pull-downs

For peptide pull-downs with nuclear extracts, 10 μl of streptavidin Sepharose beads (GE Healthcare) were saturated with 10 μg of specific histone H3 biotinylated peptides (encompassing aminoacids 10–27 of H3) for 45 minutes at 4 °C under rotation in peptide buffer (50 mM Tris pH 7.5, 150 mM NaCl, 0.1% NP-40), then washed 3 times in the same buffer. Beads were then incubated with 560 μg of HeLa cytoplasmic extract for 4 h at 4 °C under rotation in peptide buffer. Beads were then washed 3 times in the same buffer and resuspended in Laemmli buffer for immunoblot analysis.

For peptide pull-downs with recombinant proteins we followed the same protocol with the following modifications: 10 μl of Dynabeads MyOne Streptavidin T1 (Invitrogen) were saturated with 1 μg of specific histone H3 biotinylated peptides. After washes the beads were incubated with 1 μg of recombinant protein.

Northern blot

RNA purifications from nuclear and cytoplasmic fractions and northern blot were performed as previously described [33].

Supplementary Material

Refer to Web version on PubMed Central for supplementary material.

Acknowledgments

We thank O. Gozani and members of the Chua and Gozani laboratories for useful discussions, and S. Paredes, T. Hong, and L.D. Boxer for technical assistance. We thank X. Shi (University of Texas MD Anderson Cancer Center) for providing bacterial expression vectors for the AF9 YEATS domain, and Z. Yang (Stanford University) for KAP1 expression vectors. This work was supported by grants from the US National Institutes of Health (NIH) to K.F.C. (R01 AG028867, R56AG050997), the Department of Veterans Affairs to K.F.C. (Merit Award), the Paul F. Glenn Laboratories for the Biology of Aging (K.F.C), and by fellowship awards to L.T. (Italian Foundation for Cancer Research fellowship abroad, American Italian Cancer Foundation post-doctoral research fellowship, and Stanford Dean's fellowship), and to Z.O. (Walter and Idun Berry post-doctoral fellowship). Work in the W.L. laboratory was funded in part by grants from the Cancer Prevention Research Institute of Texas (RP110471-C3) and NIH (R01HG007538).

REFERENCES FOR MAIN TEXT

1. De Cecco M, et al. Genomes of replicatively senescent cells undergo global epigenetic changes leading to gene silencing and activation of transposable elements. Aging Cell. 2013
2. De Cecco M, et al. Transposable elements become active and mobile in the genomes of aging mammalian somatic tissues. Aging (Albany NY). 2013; 5:867–83. [PubMed: 24323947]
3. Ting DT, et al. Aberrant overexpression of satellite repeats in pancreatic and other epithelial cancers. Science. 2011; 331:593–6. [PubMed: 21233348]
4. Shumaker DK, et al. Mutant nuclear lamin A leads to progressive alterations of epigenetic control in premature aging. Proc Natl Acad Sci U S A. 2006; 103:8703–8. [PubMed: 16738054]
5. Shah PP, et al. Lamin B1 depletion in senescent cells triggers large-scale changes in gene expression and the chromatin landscape. Genes Dev. 2013; 27:1787–99. [PubMed: 23934658]
6. Kugel S, Mostoslavsky R. Chromatin and beyond: the multitasking roles for SIRT6. Trends Biochem Sci. 2014; 39:72–81. [PubMed: 24438746]
7. Mostoslavsky R, et al. Genomic instability and aging-like phenotype in the absence of mammalian SIRT6. Cell. 2006; 124:315–29. [PubMed: 16439206]
8. Zhong L, et al. The histone deacetylase Sirt6 regulates glucose homeostasis via Hif1alpha. Cell. 2010; 140:280–93. [PubMed: 20141841]
9. Kim HS, et al. Hepatic-specific disruption of SIRT6 in mice results in fatty liver formation due to enhanced glycolysis and triglyceride synthesis. Cell Metab. 2010; 12:224–36. [PubMed: 20816089]
10. Sebastian C, et al. The histone deacetylase SIRT6 is a tumor suppressor that controls cancer metabolism. Cell. 2012; 151:1185–99. [PubMed: 23217706]
11. Xiao C, et al. Progression of Chronic Liver Inflammation and Fibrosis Driven by Activation of c-JUN Signaling in Sirt6 Mutant Mice. J Biol Chem. 2012
12. Masri S, et al. Partitioning Circadian Transcription by SIRT6 Leads to Segregated Control of Cellular Metabolism. Cell. 2014; 158:659–72. [PubMed: 25083875]
13. Kanfi Y, et al. The sirtuin SIRT6 regulates lifespan in male mice. Nature. 2012
14. Lin Z, et al. USP10 antagonizes c-Myc transcriptional activation through SIRT6 stabilization to suppress tumor formation. Cell Rep. 2013; 5:1639–49. [PubMed: 24332849]
15. Lerrer B, Gertler AA, Cohen HY. The complex role of SIRT6 in carcinogenesis. Carcinogenesis. 2015
16. Sharma A, et al. The role of SIRT6 protein in aging and reprogramming of human induced pluripotent stem cells. J Biol Chem. 2013; 288:18439–47. [PubMed: 23653361]
17. Michishita E, et al. SIRT6 is a histone H3 lysine 9 deacetylase that modulates telomeric chromatin. Nature. 2008; 452:492–6. [PubMed: 18337721]
18. Michishita E, et al. Cell cycle-dependent deacetylation of telomeric histone H3 lysine K56 by human SIRT6. Cell Cycle. 2009; 8:2664–6. [PubMed: 19625767]
19. Yang B, Zwaans BM, Eckersdorff M, Lombard DB. The sirtuin SIRT6 deacetylates H3 K56Ac in vivo to promote genomic stability. Cell Cycle. 2009; 8:2662–3. [PubMed: 19597350]
20. Tennen RI, Bua DJ, Wright WE, Chua KF. SIRT6 is required for maintenance of telomere position effect in human cells. Nat Commun. 2011; 2:433. [PubMed: 21847107]

21. Kawahara TL, et al. SIRT6 links histone H3 lysine 9 deacetylation to NF-kappaB-dependent gene expression and organismal life span. Cell. 2009; 136:62–74. [PubMed: 19135889]
22. Sundaresan NR, et al. The sirtuin SIRT6 blocks IGF-Akt signaling and development of cardiac hypertrophy by targeting c-Jun. Nat Med. 2012
23. McCord RA, et al. SIRT6 stabilizes DNA-dependent protein kinase at chromatin for DNA double-strand break repair. Aging (Albany NY). 2009; 1:109–21. [PubMed: 20157594]
24. Toiber D, et al. SIRT6 recruits SNF2H to DNA break sites, preventing genomic instability through chromatin remodeling. Mol Cell. 2013; 51:454–68. [PubMed: 23911928]
25. Kaidi A, Weinert BT, Choudhary C, Jackson SP. Human SIRT6 promotes DNA end resection through CtIP deacetylation. Science. 2010; 329:1348–53. [PubMed: 20829486]
26. Mao Z, et al. SIRT6 promotes DNA repair under stress by activating PARP1. Science. 2011; 332:1443–6. [PubMed: 21680843]
27. Dominy JE Jr, et al. The deacetylase Sirt6 activates the acetyltransferase GCN5 and suppresses hepatic gluconeogenesis. Mol Cell. 2012; 48:900–13. [PubMed: 23142079]
28. Van Meter M, et al. SIRT6 represses LINE1 retrotransposons by ribosylating KAP1 but this repression fails with stress and age. Nat Commun. 2014; 5:5011. [PubMed: 25247314]
29. Jiang H, et al. SIRT6 regulates TNF-alpha secretion through hydrolysis of long-chain fatty acyl lysine. Nature. 2013; 496:110–3. [PubMed: 23552949]
30. Eymery A, Callanan M, Vourc'h C. The secret message of heterochromatin: new insights into the mechanisms and function of centromeric and pericentric repeat sequence transcription. Int J Dev Biol. 2009; 53:259–68. [PubMed: 19412885]
31. Gonzalez-Barrios R, Soto-Reyes E, Herrera LA. Assembling pieces of the centromere epigenetics puzzle. Epigenetics. 2012; 7:3–13. [PubMed: 22207360]
32. Gil R, Barth S, Kanfi Y, Cohen HY. SIRT6 exhibits nucleosome-dependent deacetylase activity. Nucleic Acids Res. 2013; 41:8537–45. [PubMed: 23892288]
33. Valgardsdottir R, et al. Structural and functional characterization of noncoding repetitive RNAs transcribed in stressed human cells. Mol Biol Cell. 2005; 16:2597–604. [PubMed: 15788562]
34. Martens JH, et al. The profile of repeat-associated histone lysine methylation states in the mouse epigenome. EMBO J. 2005; 24:800–12. [PubMed: 15678104]
35. Peters AH, et al. Loss of the Suv39h histone methyltransferases impairs mammalian heterochromatin and genome stability. Cell. 2001; 107:323–37. [PubMed: 11701123]
36. Rowbotham SP, et al. Maintenance of silent chromatin through replication requires SWI/SNF-like chromatin remodeler SMARCAD1. Mol Cell. 2011; 42:285–96. [PubMed: 21549307]
37. Briers S, Crawford C, Bickmore WA, Sutherland HG. KRAB zinc-finger proteins localise to novel KAP1-containing foci that are adjacent to PML nuclear bodies. J Cell Sci. 2009; 122:937–46. [PubMed: 19258395]
38. Zeng L, et al. Structural insights into human KAP1 PHD finger-bromodomain and its role in gene silencing. Nat Struct Mol Biol. 2008; 15:626–33. [PubMed: 18488044]
39. Li Y, et al. AF9 YEATS domain links histone acetylation to DOT1L-mediated H3K79 methylation. Cell. 2014; 159:558–71. [PubMed: 25417107]
40. Grewal SI. RNAi-dependent formation of heterochromatin and its diverse functions. Curr Opin Genet Dev. 2010; 20:134–41. [PubMed: 20207534]
41. Buhler M, Moazed D. Transcription and RNAi in heterochromatic gene silencing. Nat Struct Mol Biol. 2007; 14:1041–8. [PubMed: 17984966]
42. Maison C, et al. Higher-order structure in pericentric heterochromatin involves a distinct pattern of histone modification and an RNA component. Nat Genet. 2002; 30:329–34. [PubMed: 11850619]
43. Rudd NL, Williams SE, Evans M, Hennig UG, Hoar DI. Kinetochore analysis of micronuclei allows insights into the actions of colcemid and mitomycin C. Mutat Res. 1991; 261:57–68. [PubMed: 1908944]
44. Zhu Q, et al. BRCA1 tumour suppression occurs via heterochromatin-mediated silencing. Nature. 2011; 477:179–84. [PubMed: 21901007]
45. Wang Z, et al. Combinatorial patterns of histone acetylations and methylations in the human genome. Nat Genet. 2008; 40:897–903. [PubMed: 18552846]

46. Barber MF, et al. SIRT7 links H3K18 deacetylation to maintenance of oncogenic transformation. Nature. 2012; 487:114–8. [PubMed: 22722849]
47. Oberdoerffer P, et al. SIRT1 redistribution on chromatin promotes genomic stability but alters gene expression during aging. Cell. 2008; 135:907–18. [PubMed: 19041753]
48. Pinheiro I, et al. Prdm3 and Prdm16 are H3K9me1 methyltransferases required for mammalian heterochromatin integrity. Cell. 2012; 150:948–60. [PubMed: 22939622]
49. Zhang W, et al. A Werner syndrome stem cell model unveils heterochromatin alterations as a driver of human aging. Science. 2015
50. Boyarchuk E, Filipescu D, Vassias I, Cantaloube S, Almouzni G. The histone variant composition of centromeres is controlled by the pericentric heterochromatin state during the cell cycle. J Cell Sci. 2014; 127:3347–59. [PubMed: 24906798]
51. Bunch H, et al. TRIM28 regulates RNA polymerase II promoter-proximal pausing and pause release. Nat Struct Mol Biol. 2014; 21:876–83. [PubMed: 25173174]
52. Endisha H, et al. Restoring SIRT6 Expression in Hutchinson-Gilford Progeria Syndrome Cells Impedes Premature Senescence and Formation of Dysmorphic Nuclei. Pathobiology. 2015; 82:9–20. [PubMed: 25765721]
53. Todaro GJ, Green H. Quantitative studies of the growth of mouse embryo cells in culture and their development into established lines. J Cell Biol. 1963; 17:299–313. [PubMed: 13985244]
54. Valgardsdottir R, et al. Transcription of Satellite III non-coding RNAs is a general stress response in human cells. Nucleic Acids Res. 2008; 36:423–34. [PubMed: 18039709]
55. Michishita E, Park JY, Burneskis JM, Barrett JC, Horikawa I. Evolutionarily conserved and nonconserved cellular localizations and functions of human SIRT proteins. Mol Biol Cell. 2005; 16:4623–35. [PubMed: 16079181]
56. Dahl JA, Collas P. A quick and quantitative chromatin immunoprecipitation assay for small cell samples. Front Biosci. 2007; 12:4925–31. [PubMed: 17569620]
57. Ohzeki J, et al. Breaking the HAC Barrier: histone H3K9 acetyl/methyl balance regulates CENP-A assembly. EMBO J. 2012; 31:2391–402. [PubMed: 22473132]
58. Langmead B, Salzberg SL. Fast gapped-read alignment with Bowtie 2. Nat Methods. 2012; 9:357–9. [PubMed: 22388286]
59. Chen K, et al. DANPOS: dynamic analysis of nucleosome position and occupancy by sequencing. Genome Res. 2013; 23:341–51. [PubMed: 23193179]
60. Chan FL, et al. Active transcription and essential role of RNA polymerase II at the centromere during mitosis. Proc Natl Acad Sci U S A. 2012; 109:1979–84. [PubMed: 22308327]
61. Dimri GP, et al. A biomarker that identifies senescent human cells in culture and in aging skin in vivo. Proc Natl Acad Sci U S A. 1995; 92:9363–7. [PubMed: 7568133]

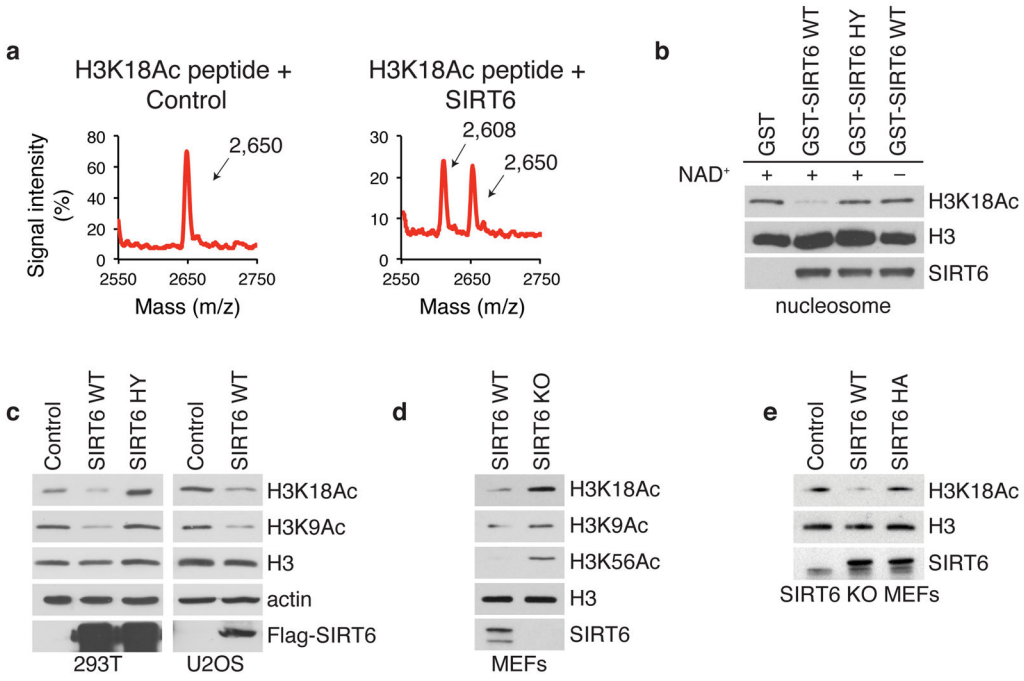

Figure 1. H3K18Ac is a physiologic SIRT6 substrate

(a) Mass spectra peak profile of H3K18Ac peptide after *in vitro* deacetylation assays with SIRT6 enzyme or in control reaction lacking enzyme. Molecular masses of acetylated and deacetylated peptides (arrows) are 2,650 and 2,608 daltons, respectively. **(b)** Western analysis showing H3K18Ac levels on nucleosomes after *in vitro* deacetylation assay. Reactions with or without NAD^+, control GST, wild-type (WT) GST-SIRT6, (GST-SIRT6 WT) or mutant GST-SIRT6 H133Y (GST-SIRT6 HY) proteins are indicated. Similar results were obtained in 4 independent experiments. **(c)** Western analysis showing H3K18Ac and H3K9Ac levels in 293T and U2OS cells overexpressing SIRT6 WT, SIRT6 HY, or control empty vector. Actin and total H3 levels are shown as controls. **(d)** Western analysis showing H3K18Ac, H3K9Ac, and H3K56Ac levels in SIRT6 knockout (KO) MEFs compared to WT littermate control MEFs. **(e)** Western analysis showing H3K18Ac levels in SIRT6 KO MEFs reconstituted with WT murine SIRT6 protein (SIRT6 WT), or a catalytically inactive H133A mutant (SIRT6 HA). Uncropped gel images are shown in Supplementary Data Set 1.

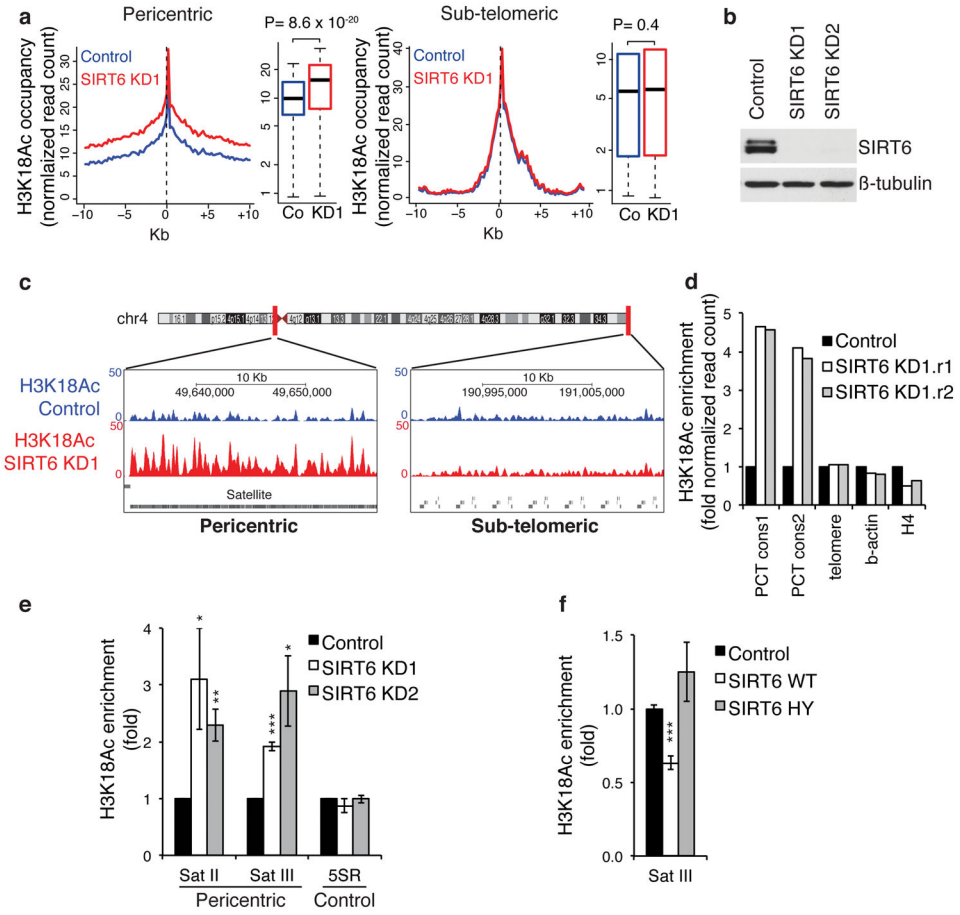

Figure 2. SIRT6 selectively regulates H3K18 deacetylation at pericentric chromatin

(a) H3K18Ac ChIP-seq analysis at pericentric and sub-telomeric heterochromatin. Genome-wide peak profiles (left) and relative box-and-whisker plots (right) show average H3K18Ac occupancy in SIRT6 knockdown (SIRT6 KD1) or control cells (Co), within 100Kb windows from centromeric gaps (Pericentric), or telomere gaps (Sub-telomeric). For box-and-whisker plots: center line is the medium value (middle quartile); top and bottom of box represent upper and lower quartile, respectively; top of upper whisker and bottom of lower whisker represent maximum and minimum, respectively (two-tailed Student's t-test, n=500 for pericentric and n=51 for sub-telomeric regions). **(b)** Western blot showing SIRT6 levels in U2OS cells upon lentiviral transduction of two independent SIRT6 shRNAs (SIRT6 KD1, SIRT6 KD2). Uncropped gel images are shown in Supplementary Data Set 1. **(c)** UCSC Genome Browser screen shots showing H3K18Ac ChIP-seq levels at representative pericentric and sub-telomeric regions of Chr4, in control and SIRT6 KD1 U2OS cells. y-axis is normalized read count. **(d)** ChIP-seq H3K18Ac levels at two pericentric consensus sequences (PCT cons1, PCT cons2) in SIRT6 KD1 and control cells. Telomeric sequences, β-actin, and histone H4 are shown as controls. Graph shows values of forward and reverse paired-end reads (r1 and r2). **(e)** ChIP-qPCR showing H3K18Ac enrichment in U2OS SIRT6 KD1 and KD2 cells at pericentric satellite Satellite II and III (Sat II, Sat III) repeats, or at control 5S ribosomal DNA (5SR) region (mean +/− s.e.m. of n=3 independent knock-down experiments). **(f)** ChIP-qPCR showing H3K18Ac enrichment in U2OS cells overexpressing

SIRT6 WT, or SIRT6 HY catalytic mutant at pericentric repeats (mean +/− s.e.m. n=4 technical replicates). Similar results were observed in 2 independent cell cultures. *p<0.05; **p<0.01; ***p<0.001; when not indicated, p>0.05 (one-tailed Student's t-test).

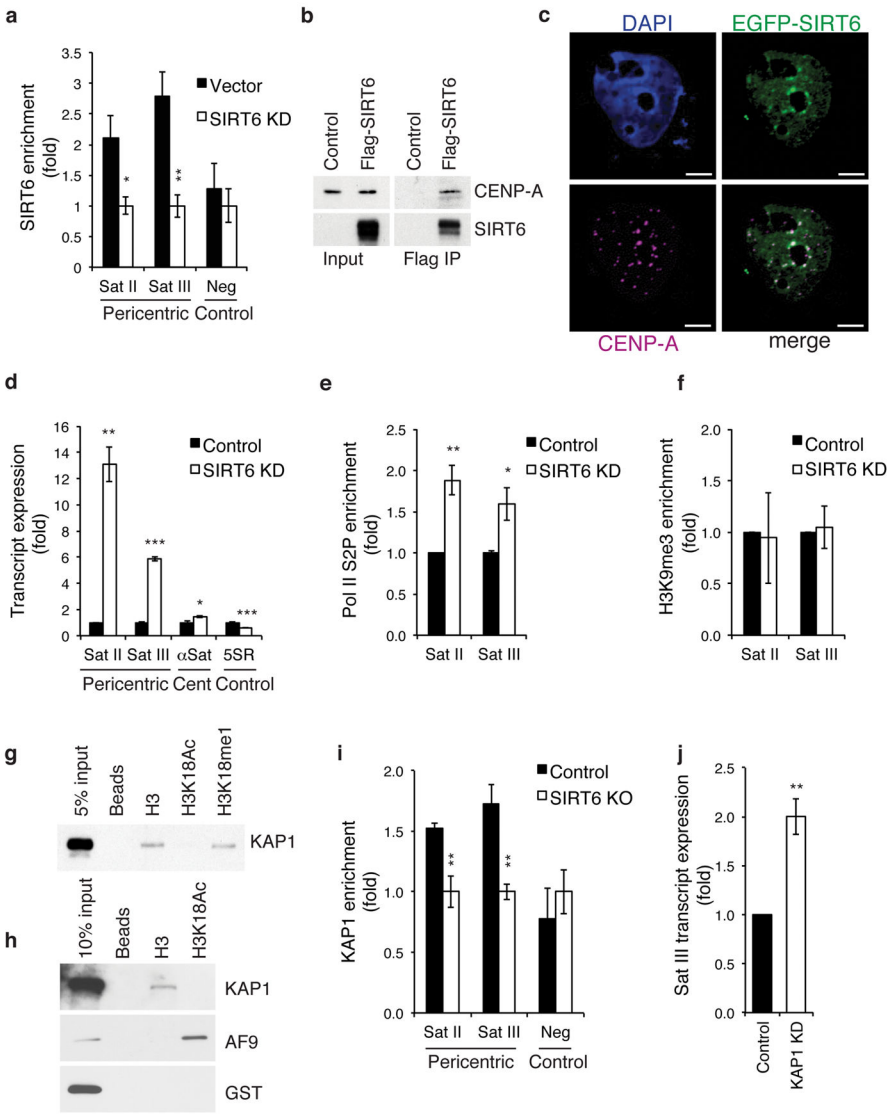

Figure 3. SIRT6-depletion disrupts pericentric chromatin silencing and leads to aberrant accumulation of satellite transcripts

(a) ChIP-qPCR showing SIRT6 occupancy at pericentric Satellite (Sat II, Sat III) repeats (mean +/− s.e.m. of n=3 technical replicates). Neg (Negative control intergenic region). Fold change represents % input of SIRT6 ChIPs normalized to values in SIRT6 knockdown cells (SIRT6 KD). **(b)** Anti-Flag immunoprecipitation (Flag IP) from nucleosome preparations from cells expressing Flag-SIRT6 or empty vector (Control). CENP-A westerns detect centromeric nucleosomes. **(c)** Representative confocal microscopy images of U2OS cells expressing EGFP-SIRT6, stained for CENP-A after *in situ* detergent extraction of nucleoplasmic protein. Bar, 5μm. **(d)** Pericentric Satellite, centromeric αSatellite (Cent, αSat), and control 5S Ribosomal RNA (5SR) transcript levels in U2OS SIRT6 KD cells, determined by qRT–PCR (mean +/− s.d. of n=3 technical replicates). **(e)** ChIP-qPCR for RNA-Pol II Ser2-phopsho (Pol II S2P) in U2OS cells (mean +/− s.e.m. of n=3 technical replicates). **(f)** ChIP-qPCR for H3K9me3 in U2OS cells (mean +/− s.e.m. of n=3

independent knockdown experiments). **(g,h)** Immunoblots of peptide pull-downs with (g) nuclear extracts or (h) recombinant proteins. The AF9 YEATS domain (which binds H3K18Ac) and GST protein are shown as controls. Peptides used encompass amino acids 10–27 of histone H3. Similar results were observed in 2 independent experiments. **(i)** ChIP-qPCR for KAP1 in control or SIRT6 knockout (SIRT6 KO) U2OS cells (mean +/− s.e.m. of n=3 technical replicates). **(j)** Pericentric Sat III transcript levels in KAP1-deficient (KAP1 KD) U2OS cells, determined by qRT–PCR (mean +/− s.e.m. of n=3 independent knockdown experiments). In (a), (d), (e), (f), (i) and (j): *p<0.05; **p<0.01; ***p<0.001; when not indicated, p>0.05 (one-tailed Student's t-test). In (a-e) and (i), results are representative of 3 different experiments from independent cell cultures. Uncropped gel images are shown in Supplementary Data Set 1.

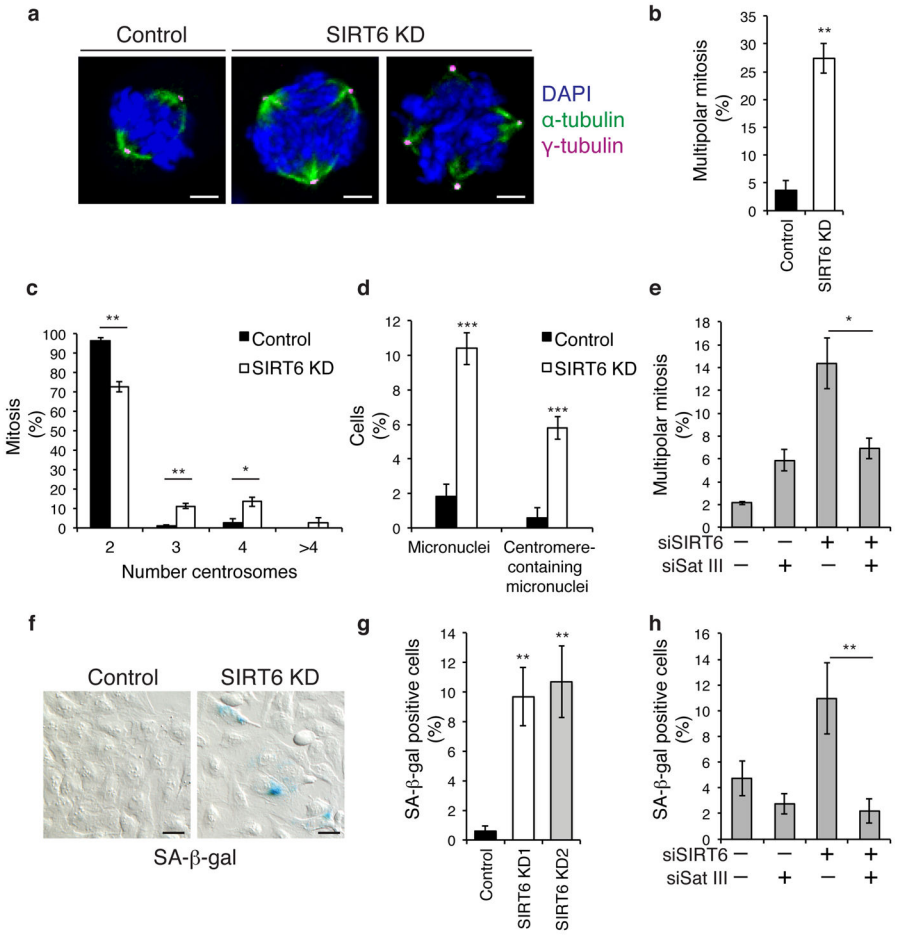

Figure 4. Aberrant accumulation of pericentric satellite transcripts in SIRT6-deficient cells causes mitotic defects and cellular senescence

(a) Representative confocal microscopy images showing multipolar mitoses in SIRT6-deficient U2OS cells compared to a bipolar normal mitosis in control cells. DNA was stained with DAPI (blue), spindle microtubules with α-tubulin (green), and centrosomes with γ-tubulin (magenta). Bar, 5 μm. **(b, c)** Quantification of multipolar mitoses (b) and centrosome numbers (c) in control or SIRT6 KD U2OS cells (mean +/− s.e.m. of n=3 independent knockdown experiments). (**d**) Quantification of U2OS cells with any micronuclei or centromere-positive micronuclei, stained as in Supplementary Fig. S4b (mean +/− s.e.m. of n=5 quantifications). (**e**) Quantification of multipolar mitoses in U2OS cells transiently transfected with siRNAs specific for SIRT6 (siSIRT6), Sat III transcripts (siSat III), and negative control siRNAs (–), as indicated (mean +/− s.e.m. of n=3 independent knockdown experiments). (**f**) Senescence-associated β-galactosidase (SA-β-gal) activity assay. Representative image of U2OS cells assayed one week after shSIRT6 or control transduction. Bar, 25 μm. **(g)** Quantification of SA-β-gal positive cells shown in (f) (mean +/− s.e.m. of n=5 quantifications). Experiment is representative of 3 independent knockdown experiments. **(h)** Quantification of SA-β-gal positive U2OS cells transfected as in (e) (mean +/− s.e.m. of n=5 quantifications). Representative images are shown in Supplementary Fig. S4d. Experiment is representative of 3 independent knockdown

experiments. In all panels, *p<0.05; **p<0.01; ***p<0.001; and when not indicated, p>0.05 (two-tailed Student's t-test).